Roca JM, Pelegrí JL, 2020. Analysis of the planetary thermal distribution with a simple three-zone maximum-flux model, International Journal of Heat and Mass Transfer.

Analysis of the planetary thermal distribution with a simple three-zone maximum-flux model

Josep Miquel Roca and Josep L. Pelegrí

Departament d'Oceanografia Física i Tecnològica, Institut de Ciències del Mar, CSIC, Unidad Asociada ULPGC-CSIC, Barcelona

Abstract

The large uncertainties in the forecasting of future global climatic conditions endorse the need of developing simple yet credible predicting tools. Here we propose a three-zone steady-state radiative model that maximizes latitudinal heat fluxes and considers the potential effect of the Earth's declination. The model is formulated as a set of five equations and six unknowns (zonal temperatures and widths, and the latitudinal heat transport) that requires specifying the reflected (albedo) and back-to-Earth (greenhouse) radiation fractions and obliges turning the low-latitude temperature into an additional parameter. The results do depend on the Earth declination, with changes of 0.5/1.5 K in the intermediate/high zones, which is interpreted as potentially affecting the greenhouse and high-latitude albedo coefficients. Therefore, we focus on identifying the effects of changes in these parameters – properly selected to represent last-glacial-maximum, modern and end-of the-century conditions. The main change is a large rise of the high-latitude temperature, favored both by a decrease in the high-latitude albedo and an increase in the greenhouse factor. For the other variables, the temporal changes in these parameters compete among them, resulting in one trend from glacial to modern times and a reversal between now and the end of the 21st century (currently a warming-narrowing of the intermediate region and the widening of both the low- and high-latitude zones); however, we note that an increase in the low-latitude temperature would tend to alleviate these changes. Despite its simplicity, the model leads to realistic global trends, becoming a useful simple tool for exploring the sensitivity of the Earth's heat distribution to changes in radiative fluxes and endorsing the validity of the maximum latitudinal-heat-transport premise.

1. Introduction

As for any complex living being, we may possibly envision the Earth as a system that has evolved in time such as to operate close to an optimum metabolic state. This simple evolutionary argument is related to the constructal theory, which states that in any complex system the flow naturally evolves towards spatial and temporal structures that optimize the transfer of energy [1-4]. Bejan and collaborators have applied this theory with substantial success to describe the operation of both living and non-living systems [5-7], included the Earth's climate [8-10].

The constructal theory does not imply that a complex system has to remain in one single state but rather that at any time the flux of energy is to be maximized, i.e. the system is in an optimized state. The system may actually revolve near one of several possible thermodynamic states (attractors), the transition taking place when certain threshold conditions are overcome [11-13]. The living Earth is a good example of this behavior, with its thermodynamics and energy balance revolving at any time near one attractor but experiencing transitions from one state to another. This behavior resembles the shifts between periods of rest and exercise that characterize all living beings: during the resting interval the system makes up reserves that are used during the exercise period [14-15].

In a simple model developed in the framework of the constructal Law, the Earth was divided in two different zones – a low-latitude warm zone and a high-latitude cold zone – and forced with the insolation received at equinox [8-10]. In the original work [8], there was no solar incoming radiation in the high-latitude compartment and dissipation was incorporated through an independent ad-hoc equation. This study was later improved by incorporating all radiative terms and by requiring that the energy flow between both compartments is maximized [9]. This provided mean temperatures of the low- and high-latitude regions but also led to different spatial coverages of both compartments, which was interpreted as if there was an intermediate zone. Finally, the model was modified to investigate how the temperature of the two compartments changes as a function of the Earth's albedo and greenhouse coefficients but the formulation led to a constant areal partition between the two regions [10].

In this work we pursue the study of the Earth's energy balance with the constructal approach, removing some of the limitations in these previous works and applying the model to forecast the Earth's changes from the last glacial maximum to the end of the 21st century. Foremost, each hemisphere is segmented into three geographical zones, connected using a criterion of energy-flow maximization. The requirement is that the intermediate region is in radiative balance, a fairly reasonable approximation for much of the mid-latitude areas of the world. This provides a consistent partition into three zones and defines a constant energy flow between the three compartments. Further, our formulation incorporates the Earth's declination, which allows exploring how the energy budget depends on using either the radiative forcing at a certain specific time (e.g. the equinox) or having the year-long mean radiation. The results show that there are significant differences, which are interpreted as giving rise to feedback mechanisms that may affect the albedo and greenhouse factors. Hence, we place our emphasis on setting the model's parameters for the last glacial maximum, modern and future conditions; in particular, we develop a simple procedure that allows us estimating the time evolution of the greenhouse factor. The model is finally applied for a range of albedo and greenhouse coefficients, in order to investigate the long-term variations between the different thermodynamic states.

The article is structured as follows. In section 2 we introduce the model, explaining the fundamental ideas behind the three-zone partition and developing the model's energy equations. In section 3 we address the difficult task of setting the models' parameters – albedo, greenhouse effect, low-zone temperature and effective declination – and in section 4 we illustrate the dependence of the results on these parameters. We conclude in section 5 with a discussion of the model's predictions about the evolution from past glacial to present and future scenarios plus some final considerations on optimal fluxes in the living Earth.

2. The model

2.1. Main assumptions and three-zone latitudinal partition

The solar radiation at origin is approximately constant but the amount of heat arriving to the Earth's surface is a function of latitude and time. The radiation arriving at any

site changes throughout the year because of the Earth's translation around the Sun and because of three main astronomical movements (eccentricity, obliquity and precession) that set the Earth-Sun distance and the orientation of the Earth's axis of rotation with respect to the plane formed by the Earth-Sun system (ecliptic).

Among these three astronomical motions, obliquity is the principal one responsible for changes in the annual-mean insolation at any site, and therefore will be the only one considered in this study. Obliquity sets the (solar) declination (φ) – the angle between the ecliptic and the Earth's axis of rotation – which changes by as much as 5° with a periodicity close to 41,000 yrs. The energy effectively arriving to the Earth's surface also depends on the fraction of the incoming radiation that is reflected, an effect known as the albedo α (section 3.1). The outgoing long-wave radiation depends not only on the temperature of the Earth but also on the greenhouse gases (section 3.2), whose net effect is the back-radiation of some of this long-wave heat flux (a fraction λ, known as the greenhouse factor).

The model considers latitudinal rings englobing the entire Earth, hence ignoring any longitudinal variations. Further, it assumes the Earth to be in steady state, i.e. the forcing remains constant long enough for the Earth system to stabilize (be close enough to a thermodynamic attractor). The steady state is a fair assumption if we are to consider only the 40,000-years periodicity but is certainly not adequate for the seasonal cycle (section 3.4). The model further idealizes the Earth as split in three latitudinal bands – low, intermediate and high – based on a simple criterion for the sign of the net radiation (short-wave solar ingoing minus long-wave outgoing) (Fig. 1). In the low zone, which represents the equatorial and tropical latitudes, the ingoing exceeds the outgoing radiation. The intermediate zone corresponds to temperate areas, where the ingoing and outgoing radiative fluxes (energy per unit area and time) are fairly similar so we impose the net radiation to be zero; actual observations show that there is a latitudinal band as wide as 20° where the difference is less than 20% [16-17]. The high zone matches the subpolar and polar regions, with long-wave outgoing fluxes exceeding the ingoing solar input. Within each zone, the temperature is set constant, with the low-latitude temperature chosen as a model parameter (section 3.3) and the temperatures of the other zones being two of the five output

variables. The other three output variables are the latitudinal heat flux and the latitudes separating the low-intermediate and intermediate-high zones.

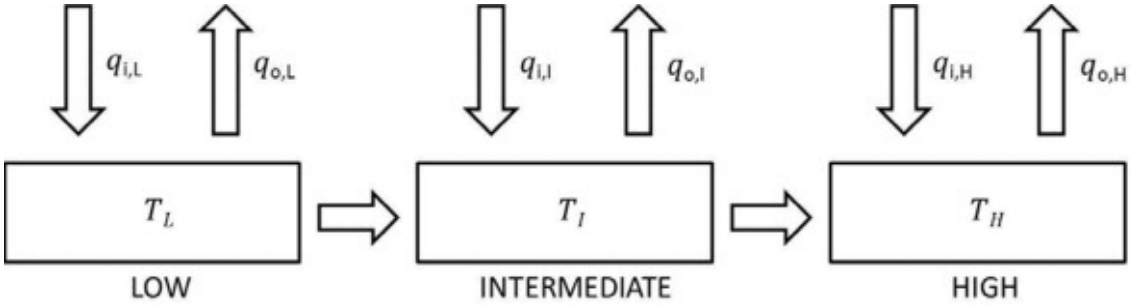

Figure 1. Segmentation of one hemisphere into three zones, showing the incoming solar radiation, outgoing long-wave radiation and energy transports between the zones.

The greenhouse factor is set constant for the entire Earth but the albedo is let to vary from one zone to another, depending on the amount of clouds, the water fraction coverage and the type of land coverage (sections 3.1 and 3.2). As a result, our model includes six parameters: the low-latitude temperature, the solar declination angle, the greenhouse factor and the albedos (one for each zone).

Finally, the model allows heat transport to occur between two adjacent zones. Rather than calculating the advective and diffusive fluxes (per unit time and area) we consider the meridional transport after integration over the entire globe along a constant-latitude plane. These transports, which result from the heat balance in the two adjacent zones, are maximized as a function of the latitudinal limits of these zones. This maximization closes the system and constitutes the practical expression of the constructal law.

Nomenclature

σ	Stefan-Boltzmann constant (5.67×10^{-8} W m^{-2} K^{-4})
T_s	solar temperature (5762 K)
R	equivalent radius of the Earth (6371 km)
F	Sun-Earth vision factor, 2.16×10^{-5}
q	energy per unit time into or out of each compartment (W)
θ	latitude
θ_L	upper latitude and width for the low-latitude zone

θ_I	upper latitude for the intermediate-latitude zone
$\theta_I - \theta_L$	width of the intermediate-latitude zone
θ_H	width of the high-latitude zone
T	temperature (K)
α	albedo
φ	solar declination angle
λ	greenhouse factor

Subindexes (but see nomenclature above for specific latitudinal notation)

L	low-latitude zone
I	intermediate-latitude zone
H	high-latitude zone
LI	refers to exchange between low and intermediate zones
IH	refers to exchange between intermediate and high zones
i	refers to ingoing short-wave solar radiation, e.g. the subindex pair *i,L* would refer to ingoing radiation in the low-latitude zone
o	refers to outgoing long-wave radiation, e.g. the subindex pair *o,H* would refer to outgoing radiation in the high-latitude zone

2.2. Model equations

We consider the heat balance for the northern hemisphere; the situation in the southern hemisphere would be analogous but with a phase difference of six months. The variables characterizing the partition of the hemisphere in three zones are illustrated in Figure 2. The zonal bands are delimited by several latitudes, as follows: the equator and θ_L for the low zone, $\theta_L$and θ_I for the intermediate zone, and θ_I and $\pi/2 + \varphi$ for the high zone.

The radiation per unit area that reaches any latitude θ is proportional to the radiation per unit area arriving to a plane normal to the ecliptic and to the local orientation of the Earth's surface with respect to the ecliptic, $\cos(\theta - \varphi)$. Hence, for a zonal ring that encircles the Earth – located at a latitude θ, of width $d\theta$, and with temperature T – the radiation captured (in) and emitted (out) are

$$q_i = 2R^2 F\left(1-\alpha\right)\sigma T_s^4 \cos\theta \cos\left(\theta-\varphi\right) d\theta \quad (1)$$

$$q_o = 2\pi R^2 \left(1-\lambda\right)\sigma T^4 \cos\theta \, d\theta \quad (2)$$

where R is the Earth's radius, σ is the Stefan-Boltzmann constant, T_s is the temperature of the Sun, α is the albedo and λ is the greenhouse factor, and the temperature is expressed in Kelvin degrees.

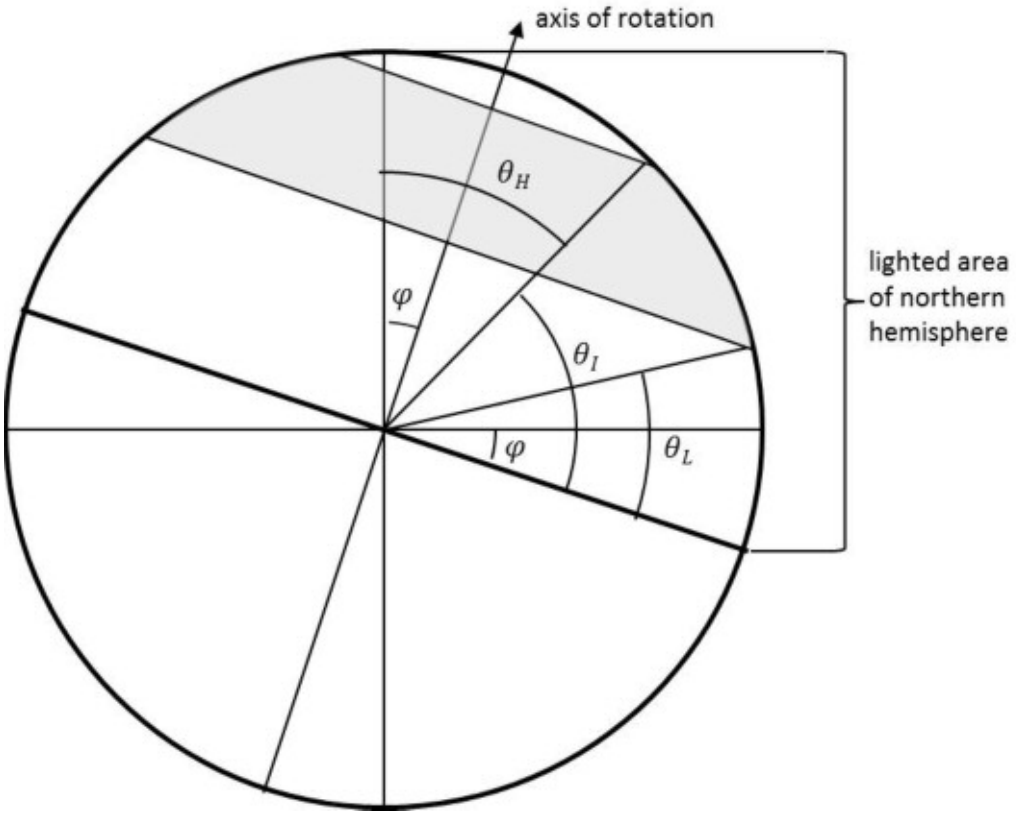

Figure 2. Latitudinal variables of the three-zone model (northern hemisphere and summer). The shaded area represents the intermediate zone and the horizontal line represents the plane of the ecliptic.

The steady-state heat balance for the low, intermediate and high zones are (Fig. 1)

$$q_{i,L} - q_{o,L} - q_{LI} = 0 \quad (3)$$

$$q_{i,I} - q_{o,I} + q_{LI} - q_{IH} = 0 \quad (4)$$

$$q_{i,H} - q_{o,H} + q_{IH} = 0 \quad (5)$$

Inserting expressions (1) and (2) for ingoing and outgoing radiation, and integrating latitudinally over each band, we have the heat balance for each zone; for the low one:

$$Y_L\left(\theta_L\cos\varphi+\sin\theta_L\cos(\theta_L-\varphi)\right)-T_L^4\sin\theta_L-\frac{q_{LI}}{2\pi R^2\sigma(1-\lambda)}=0\,, \tag{6}$$

where $Y_L=\dfrac{F}{2\pi}\dfrac{1-\alpha_L}{1-\lambda}T_S^4$; (7)

for the intermediate zone:

$$Y_I\left((\theta_I-\theta_L)\cos\varphi+\cos(\theta_I+\theta_L-\varphi)\sin(\theta_I-\theta_L)\right)-T_I^4\left(\sin\theta_I-\sin\theta_L\right)-\frac{q_{IH}-q_{LI}}{2\pi R^2\sigma(1-\lambda)}=0\,, \tag{8}$$

where $Y_I=\dfrac{F}{2\pi}\dfrac{1-\alpha_I}{1-\lambda}T_S^4$; (9)

and for the high zone:

$$Y_H\left(\left(\frac{\pi}{2}+\varphi-\theta_L\right)\cos\varphi-\sin\theta_L\cos(\theta_L-\varphi)\right)-T_H^4\left(1+\sin\varphi-\sin\theta_I\right)+\frac{q_{IL}}{2\pi R^2\sigma(1-\lambda)}=0\,, \tag{10}$$

where $Y_H=\dfrac{F}{2\pi}\dfrac{1-\alpha_H}{1-\lambda}T_S^4$, (11)

or, using $\theta_H=\dfrac{\pi}{2}+\varphi-\theta_I$, (12)

$$Y_H\left(\theta_H\cos\varphi-\sin\theta_H\cos(\theta_H-\varphi)\right)-T_H^4\left(1+\sin\varphi-\cos(\theta_H-\varphi)\right)+\frac{q_{IH}}{2\pi R^2\sigma(1-\lambda)}=0\,. \tag{13}$$

These zonal energy balances provide expressions for the meridional heat transports between adjacent zones. Following the constructal law, we ask these meridional transports to be maxima; between the low and intermediate zones:

$$\frac{\partial q_{LI}}{\partial\theta_L}=0,\quad \frac{\partial^2 q_{LI}}{\partial\theta_L{}^2}<0\,, \tag{14}$$

which implies $\dfrac{T_L^4}{Y_L}=2\cos(\theta_L-\varphi)$ and $\dfrac{T_L^4}{Y_L}<\dfrac{2\sin(2\theta_L-\varphi)}{\sin\theta_L}$; (15)

and between the intermediate and high zones:

$$\frac{\partial q_{IH}}{\partial\theta_I}=0,\quad \frac{\partial^2 q_{IH}}{\partial\theta_I{}^2}<0\,, \tag{16}$$

which gives $\dfrac{T_H^4}{Y_H}=2\cos(\theta_I-\varphi)=2\sin\theta_H$ and $\dfrac{T_H^4}{Y_H}<\dfrac{2\sin(2\theta_I-\varphi)}{\sin\theta_I}=\dfrac{2\sin(2\theta_H-\varphi)}{\cos(\theta_H-\varphi)}$. (17)

A third condition, which comes from the zero radiative balance in the intermediate zone, is $q_{LI} = q_{IH} \equiv q$.

(18)

Summarizing, the set of equations to be solved is

$$\left(\theta_L \cos\varphi + \sin\theta_L \cos(\theta_L - \varphi)\right) - \frac{T_L^4}{Y_L}\sin\theta_L - \frac{q}{2\pi R^2 \sigma(1-\lambda)Y_L} = 0, \quad (19)$$

$$Y_I\left((\theta_I - \theta_L)\cos\varphi + \cos(\theta_I + \theta_L - \varphi)\sin(\theta_I - \theta_L)\right) - \frac{T_I^4}{Y_I}\left(\sin\theta_I - \sin\theta_L\right) = 0, \quad (20)$$

$$\left(\pi/2 + \varphi - \theta_L\right)\cos\varphi - \sin\varphi\cos(\theta_L - \varphi) - \frac{T_H^4}{Y_H}\left(1 + \sin\varphi - \sin\theta_I\right) + \frac{q}{2\pi R^2 \sigma(1-\lambda)Y_H} = 0, \quad (21)$$

$$\frac{T_L^4}{Y_L} = 2\cos(\theta_L - \varphi), \quad (22)$$

$$\frac{T_H^4}{Y_H} = 2\cos\left(\theta_I - \varphi\right), \quad (23)$$

$$\theta_H = \frac{\pi}{2} + \varphi - \theta_I. \quad (24)$$

The model reduces to these six equations with seven variables or unknowns: the heat flow between zones, the three zonal temperatures and the widths of the three zones. The model parameters are the albedo, greenhouse factor and solar declination; since we have one variable in excess of the number of equations, we set the low-zone temperature as an additional known parameter.

2.3. Numerical procedure

We solve numerically the system of equations (19) to (24) as follows: (i) assign values for the albedos α_L, α_I and α_H, the greenhouse effect λ, the solar declination φ, and the tropical temperature T_L; (ii) use the definitions (7), (9) and (11) to calculate Y_L, Y_I and Y_H; (iii) use equation (22) to calculate θ_L; (iv) solve for θ_I in the equation obtained as follows: clear for q in equations (19) and (21), equate them, and replace T_H in terms of θ_I using equation (23); (v) use equation (24) to obtain θ_H; (vi) calculate T_I from equation (20); and (vii) employ equation (23) to determine T_H.

3. Model parameters

We apply the model to simulate the Earth's energy balance during the last glacial maximum, the modern conditions and two fossil-fuel-emission scenarios by the end of the 21st century. The modern conditions have changed so rapidly that we will explore the sensitivity of the model to the parameters representing the preindustrial conditions (here taken as the oldest instrumental records, essentially the 19th century), the 1951-1980 mean values (which are often taken as a reference for calculating temperature anomalies) and the most recent available data (2018-2019) [18-21]. For the conditions at the end of the 21st century we will use the predictions for the RCP6.0 and RCP8.5 scenarios of greenhouse-gases emission, which respectively reflect intermediate and relatively high greenhouse concentrations [18]; nevertheless, recent reports point at RCP8.5 as a feasible future scenario [22].

3.1. Albedo

The albedo varies greatly with latitude because of the type of soil/vegetation, the amount of cloud coverage and the changing fraction of land-ocean [23]; this last effect is also an important cause for differences between the northern and southern hemispheres. Zonally-averaged albedos change largely with latitude, with minimum/maximum values in tropical/polar regions [23-27]. On the basis of these studies, we take the current albedos for the northern hemisphere as 0.30, 0.32 and 0.60 for the low, intermediate and high zones, respectively.

Albedo has certainly changed along the Earth's paleoclimatic history, although the major changes would have happened at high latitudes as a result of changes in ice coverage. Hence, for our analysis we assume that the albedo in low and intermediate zones has not changed but will allow for albedo variations in the high-latitude zone. In particular, we will consider the last glacial maximum and modern conditions in order to characterize the glacial-interglacial transitions and will also ponder the possible conditions at the end of the XXI century. Specifically, we consider α_H to have changed between 0.85 (maximum glacial, with the entire high-latitude zone covered by snow and ice), 0.60 (modern) and 0.50 (end-of-the-century) (Table 1) [28,29].

Table 1. Earth's carbon dioxide atmospheric concentration, annual-global average surface temperature and corresponding greenhouse factors and high-latitude albedo for last-glacial-maximum, modern and end-of-the-century conditions

		CO_2 (ppm)	**Average T**	**Greenhouse factor λ**	**High-latitude albedo α_H**
Last glacial maximum		180	7.9 °C (281.05 K)	0.382	0.85
Modern	Preindustrial	280	13.8 °C (286.95 K)	0.375	0.60
	1951-1980	320	14.0 °C (287.15 K)	0.381	0.60
	2019	405	15.0 °C (288.15 K)	0.388	0.60
End of the century		670 (RCP6.0) 930 (RCP8.5)	16.6 °C (289.75 K) 18.3 °C (291.45 K)	0.406 0.413	0.50 0.50

3.2. Greenhouse effect

The greenhouse factor represents the fraction of the outgoing long-wave radiation that, because of the presence of greenhouse gases, cannot cross the atmosphere and is hence radiated back to the Earth's surface layers; the short residence time of air/gases in the atmosphere allows having one single greenhouse factor for all three latitudinal zones. The underlying assumption is that, on average, the Earth' surface is in radiative equilibrium. In such equilibrium, the difference between the mean short-wave radiation that crosses the atmosphere, S, and the mean long-wave radiation emitted by the Earth's surface, $L = \sigma T^4$, is the greenhouse long-wave back radiation, which is expressed as a fraction λ of the latter, $G = \lambda \sigma T^4$; in these expressions T is the (globally and annually) average temperature of the Earth's surface

Short-wave radiative estimates are 340.2 W m^{-2} arriving to the outer atmosphere and 100.0 W m^{-2} reflected back to space (albedo), leaving 240.2 W m^{-2} that reach the sea surface [30,31]. Therefore, in radiative equilibrium

$$S + G = L \quad \rightarrow \quad S + \lambda \sigma T^4 = \sigma T^4 \,, \tag{25}$$

where S = 240.2 W m^{-2} is the short-wave radiation arriving to the Earth's surface. From this last equation – during preindustrial conditions, T = 286.95 K (13.8 °C) – the greenhouse back-radiation was 144.2 W m^{-2} and the greenhouse factor was λ = 0.375.

In order to obtain λ values for past and future scenarios, we require knowing how $G(t)$ has evolved in time. For this purpose, we use an empirical relation that relates changes in the concentration of carbon dioxide in the atmosphere $C(t)$ with changes in the radiative forcing relative to all greenhouse gases [32,33], referenced to the preindustrial value of G_0 =144.2 W m^{-2},

$$G(t) = G_0 + A\, log\left(\frac{C(t)}{C_0}\right), \tag{26}$$

where A = 20.5 W m^{-2} and C_0 = 280 ppm.

Hence, equation (26) gives the greenhouse back-radiation values $G(t)$ from the carbon dioxide time series $C(t)$ [18,21,34,35]. Adding the temperature values $T(t)$ [18-20,36,37], the corresponding greenhouse factors $\lambda(t)$ are obtained from $G = \lambda\sigma T^4$ (Table 1). For the end-of-the-century values we have used the mean temperatures and carbon dioxide concentrations provided by the RCP6.0 and RCP8.5 scenarios.

3.3. Low-zone temperature

Our model has six equations (equations 19-24) and seven variables $(T_L, T_I, T_H, \theta_{L,}\theta_{I,}, \theta_H, q)$. By setting a value for one variable, i.e. by turning it into a parameter, we can obtain the corresponding family of solutions. The variable chosen is the temperature of the low zone, the principal reason being its stability from the preindustrial era to nowadays [38], and even between glacial and interglacial periods [39]; further, the tropics are the area of the globe that will experience the smallest changes in the end-of-the-century projections [18].

Asides its temporal stability, the sea-level temperature is fairly constant within a latitudinal band encompassing latitudes less than 15°, with values ranging between 26 and 27 °C [17,38]. This is confirmed by the monthly temperature data from 21 cities at latitudes less than 20° [40]; after removing the single hottest and coldest cities, we have an average monthly-mean temperature of 26.9°C and a median monthly-mean temperature of 27.3°C. Further, considering the monthly maximum/minimum temperatures, the average values are 28.9/26.6 °C and the median values are 28.7/26.8 °C. Therefore, for our study we will use a low-zone temperature of 300 K and will explore the sensitivity of the solution to variations from 297 to 303 K.

3.4. Effective solar declination

The tilt of the Earth's rotation axis with respect to the ecliptic is known as the declination φ, its present value being 23.45° (0.409 radians). The declination oscillates with a relatively long period (about 41,000 years) – in an astronomical movement known as obliquity – with its amplitude changing between minimum and maximum values of 22.1° (0.386 radians) and 24.5° (0.428 radians).

The major consequence of the declination is the appearance of seasonality. Further, because of the varying declination, the latitudinal distribution of the annual-mean solar radiation changes substantially during the obliquity cycle. Hence, the total yearly radiation received by the Earth remains nearly unchanged but the amplitude of the declination sets the character of seasonality, leading to significant differences between winters or summers throughout the obliquity cycle, e.g. moderate high-latitude summers and winters will occur during minimum declination values while the extreme high-latitude summers and winters will develop during the maximum declination conditions.

The model equations are not linear – in particular the outgoing radiation changes with the fourth power of the temperature – so the year-integrated energy balance for each zone (and the entire Earth) will depend on the actual declination. In Figure 3 we present the model's solution for the entire range (-0.428 radians $\leq \varphi \leq$ 0.428 radians) of declination values. The results may be understood as the conditions in a northern hemisphere that was permanently experiencing one single season, e.g. an extreme hot summer with $\varphi = 0.428$ or a mild winter with $\varphi = -0.386$. Obviously, this is an unrealistic situation but the purpose of this plot is to illustrate the character of the model's response with the objective of viewing if the actual declination value could have some effect on the year-long integrated variables.

The results show that the variables are not symmetric with respect to zero declination, particularly for the temperature of the intermediate- and high-latitude zones. Hence, we expect that the year-long integrated results will not be the same for maximum or minimum declination values; in particular, the annual-integrated response may not correspond to the steady-state response for equinox, i.e. when the plane of the Earth's equator reaches the Sun (equivalent to an instantaneous situation of zero declination).

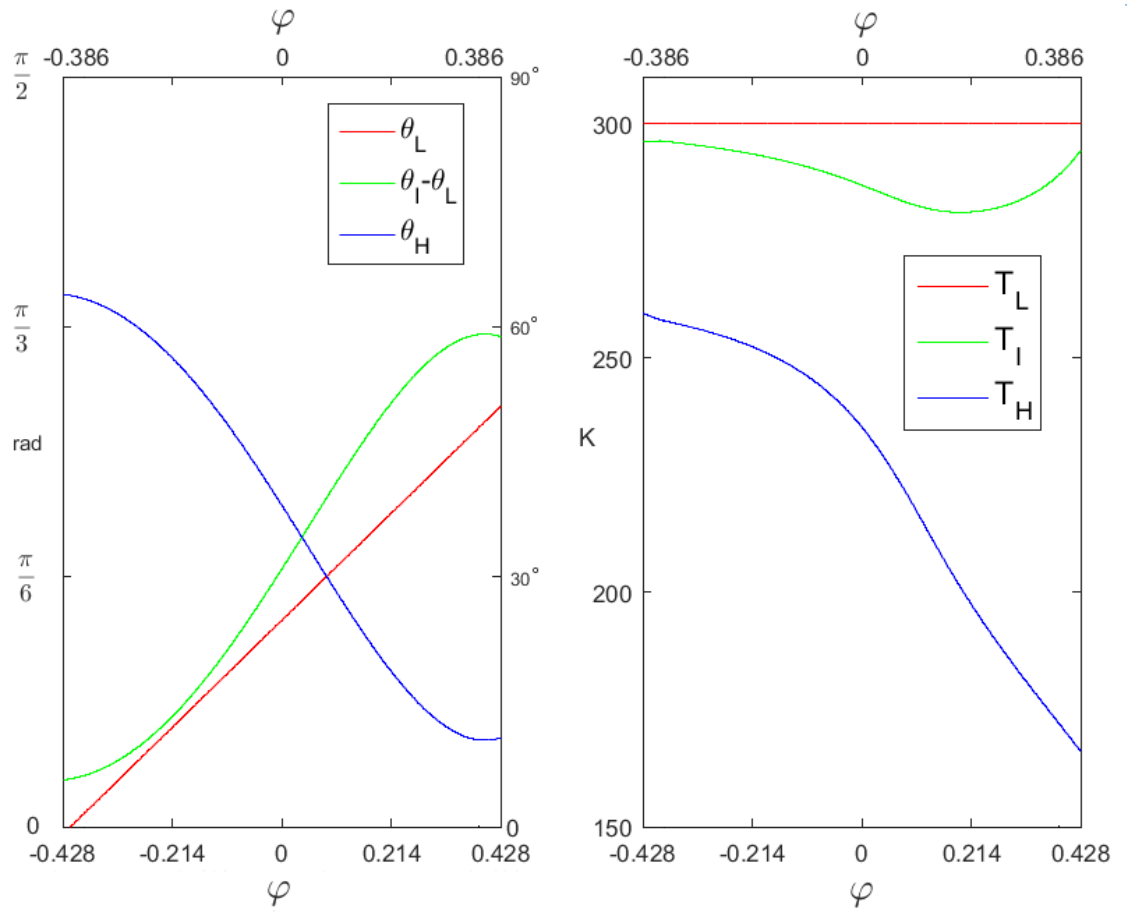

Figure 3. Dependence of the latitudinal widths and temperatures of all three zones on declination φ (the results correspond to $\alpha_L = 0.30$, $\alpha_I = 0.32$, $\alpha_H = 0.60$, $\lambda = 0.388$, and $T_L = 300$ K).

We face the task of estimating an effective declination, defined as the declination that would lead to conditions similar to the annual-integrated values. Given the model's important simplifications (e.g. assumption of steady-state radiative balance at any time of the annual cycle), we follow an elementary procedure. At any time of the year, the apparent declination is given by:

$$\psi = \psi(t) = \varphi\, sin(\omega t) = \varphi\, sin\left(\frac{2\pi t}{\tau}\right) \qquad (27)$$

where τ is one year; hence $d\psi = \left(\frac{2\pi}{\tau}\right)\varphi\, cos\left(\frac{2\pi t}{\tau}\right)$.

The mean value of the product of declination and any variable between the March and September equinoxes, for example for the latitude θ of any zone, is given by:

$$\overline{\theta\psi} \equiv \frac{2}{\tau}\int_0^{\tau/2} \theta(t)\,\psi(t)\,dt = \bar{\theta}\frac{2}{\tau}\int_0^{\tau/2} \psi(t)\,dt = \bar{\theta}\,\frac{2}{\tau}\int_0^{\tau/2} \varphi\, sin\left(\frac{2\pi t}{\tau}\right) dt = \frac{2\varphi\bar{\theta}}{\pi} \qquad (28)$$

where the zero time corresponds to the March equinox and the overbars represent mean values.

Therefore we can define an effective declination between the March and September equinoxes, $\bar{\psi} = 2\varphi/\pi$, such that $\overline{\theta\psi} \equiv \bar{\theta}\bar{\psi}$. Repeating this procedure for the other half of the year, starting on the September equinox, leads to the same absolute declination but with opposite sign. Hence, a first-order estimate of the actual year-long average is obtained by calculating the mean between the model's predictions for $\overline{\psi_1} = 2\varphi/\pi$ and $\overline{\psi_2} = -2\varphi/\pi$.

4. Results

In this section we explore the model's sensitivity to the different parameters. As a reference case, we consider the following set of parameters: $\alpha_L = 0.30$, $\alpha_I = 0.32$, $\alpha_H = 0.60$, $\lambda = 0.388$, and $T_L = 300$ K (the modern 2019 conditions in Table 1). In section 4.1 we explore the potential limitations behind using the equinox radiative conditions, in section 4.2 we examine the relevance of changes in the low-zone temperature and in section 4.3 we investigate the dependence of the solution on the greenhouse factor and the high-zone albedo.

4.1. Dependence on effective declination

In Table 2 we present, using the reference set of parameters, the temperatures of the intermediate- and high-latitude zones for maximum and minimum declination values. We show the results (i) considering equinox forcing, (ii) after linearly averaging the response over the entire range of apparent declinations and (iii) using the effective declination procedure presented in section 3.4. We focus here on the temperature changes simply because the low-intermediate and intermediate-high latitudinal limits change by less than 1° (the actual values are presented in the following sections).

Remarkably, the temperatures change depending on the selected method. In particular, for a certain declination value, those methods that consider the effect of the declination show results that can differ substantially from the calculations at equinox (which do not consider the declination). For example, using the effective declination method shows higher temperatures at intermediate latitudes (1.0-1.5 K

warmer) and lower temperatures at high latitudes (12.3-13.8 K cooler). Further, and most important, the methods that consider declination are sensitive to the actual declination value. For example, for the effective declination method, the intermediate-latitude zone warms about 0.5 K and the high-latitude zone cools some 1.5 K during maximum as compared with minimum declination.

Table 2. Temperature in the intermediate- and high-latitude zones during equinox, linearly averaged over the entire range of declination values and using the methodology described in section 3.4 ($\alpha_L = 0.30$, $\alpha_I = 0.32$, $\alpha_H = 0.60$, $\lambda = 0.388$ and and $T_L = 300$ K).

Variables	**Equinox**	**Minimum declination values -0.386 rad $\leq \varphi \leq$ 0.386 rad**		**Maximum declination values -0.428 rad $\leq \varphi \leq$ 0.428 rad**	
		Linear average	Effective declination	Linear average	Effective declination
T_I	286.9	288.0	287.9	288.6	288.4
T_H	235.3	226.2	223.0	225.0	221.5

For the remaining of this article, we consider the equinox steady-state results to be a first-order approximation to the true solution and explore the sensitivity of the results to all other three parameters. This approximation was already used by previous works that explored the constructal approach [8-10]. We also follow this approach because we believe it is coherent with the simplicity of our model and because neither the linearly-averaged nor the effective declination methods are fully accurate. Nevertheless, the above results point at two important considerations: (1) there is some significant dependence on declination; (2) the equinox declination will lead to results that overestimate the temperature values for the high-latitude zone.

4.2. Dependence on low-latitude temperature

In section 3.3 we argued that the low-zone temperature is a fairly stable variable, which can be set as a model parameter. Nevertheless, it is convenient to explore the sensitivity of the solution to this parameter, investigating what are the implications of imposing lower or greater outgoing radiation at low latitudes. In this section we explore the 297 K $\leq T_L \leq$ 303 K range (Fig. 4).

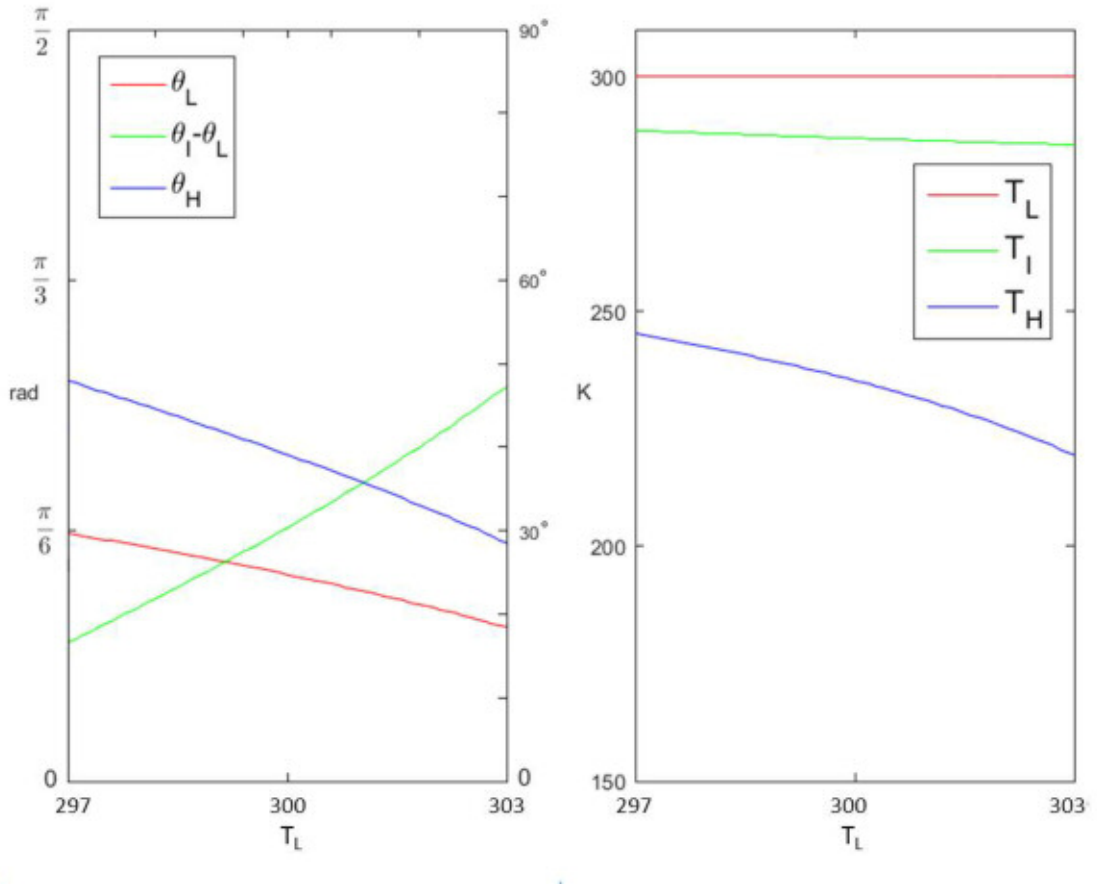

Figure 4. Dependence of the latitudinal widths and temperatures of all three zones on the low-zone temperature T_L (the results correspond to $\alpha_L = 0.30$, $\alpha_I = 0.32$, $\alpha_H = 0.60$ and $\lambda = 0.388$).

When using nowadays albedo and greenhouse factors, the model suggests that a progressive increase in the temperature of the low-latitude zone leads to an increase in the width of the intermediate zone at the expense of the other two zones. However, the combined low and intermediate zones experience a significant increase, about 20° over the entire explored range. Further, as the tropical region warms, the temperature of the intermediate zone decreases slightly (4 K) and the temperature of the high zone

is reduced by as much as 25 K. This suggests that warmer tropical areas will translate into wider and moderately warmer intermediate regions and much narrower (its width decreasing from about 49° to 29°) and colder circles near the poles.

For nowadays α_H and λ conditions, increasing T_L from 297 to 303 K is reflected in a 3.8 K increase in the Earth's average temperature. This same T_L variation, however, would have led to an increase in the average temperature of the Earth of about 30 K when using glacial coefficients but only 1.3 K if using end-of-the-century coefficients (Table 3). This reflects a decrease in the sensitivity of the solution to T_L as the greenhouse factor (albedo) increases (decreases) in high latitudes, which grants certain confidence to the predictive skill of the model for future scenarios.

Table 3. Earth's average temperature $\overline{T}$ (K) and latitudinal heat transport q (PW) for last-glacial-maximum, modern and end-of-the-century conditions as a function of the low-zone temperature T_L; the results correspond to equinox forcing for the reference scenario (α_L= 0.30, α_I =0.32, α_H =0.60 and λ = 0.388).

		$T_L = 297$ K		$T_L = 300$ K		$T_L = 303$ K	
		$\overline{T}$ (K)	q (PW)	$\overline{T}$ (K)	q (PW)	$\overline{T}$ (K)	q (PW)
Last glacial maximum		248.5	2.0	267.4	0.9	280.2	0.2
Modern	Preindustrial	278.7	1.7	280.6	0.7	282.8	<0.1
	1951-1980	279.1	2.0	280.8	0.9	282.8	0.1
	2019	279.2	2.3	281.1	1.2	283.0	0.3
End of the century (RCP6.0)		284.0	3.2	284.7	1.9	285.3	0.9

In Table 3 we have also included the low-intermediate and intermediate-high latitudinal heat transport q. When all other parameters remain constant, the results show that this transport increases as we decrease T_L, reflecting the incapacity of the low-latitude band to radiate out heat. For T_L decreasing between 300 and 297 K, the latitudinal transport increases from 1.2 to 2.3 PW, which is not far from observed values of the mean latitudinal heat transport (about 3 PW) [41].

4.3. Dependence on albedo and greenhouse factor

Our model, despite its simplicity, can help us explore how the extension and temperature of the three zones depend on the high-latitude albedo and the greenhouse factor (as argued in section 3.1, we maintain constant values for the low- and intermediate-latitude albedos: $\alpha_L = 0.30$, $\alpha_I = 0.32$). Considering first the reference scenario (Table 4), we find that the low zone occupies a strip above and below the equator of approximately 0.413 radians (23.7°), which is very close to the inclination of the Earth's axis (23.45°) that defines the latitude of parallels in the tropics of Capricorn and Cancer (approximate boundaries of the tropical climate). The intermediate zone reaches until about 54°, so that the latitudinal widths of the intermediate and high zones are some 29° and 37°, respectively. We may conclude that the model reflects reasonably well, from a geographical point of view, the Earth's latitudinal climatic zones.

Table 4. Temperature, widths and limits of the low, intermediate and high-latitude zones, considering the equinox forcing for the reference scenario ($\alpha_L = 0.30$, $\alpha_I = 0.32$, $\alpha_H = 0.60$, $\lambda = 0.388$, and $T_L = 300$ K).

Zone	**Upper-latitude limit in radians (degrees inside parenthesis)**	**Width in radians (degrees inside parenthesis)**	**Temperature (K)**
Low	$\theta_L = 0.413$ (23.7°)	$\theta_L = 0.413$ (23.7°)	300.0
Intermediate	$\theta_I = 0.919$ (53.7°)	$\theta_I - \theta_L = 0.506$ (29.0°)	286.9
High	$\theta_I + \theta_H = 1.571$ (90.0°)	$\theta_H = 0.652$ (37.4°)	235.3

We may now proceed to explore how the model results depend on the greenhouse factor and the high-latitude albedo. In Figure 5 we present the intermediate- and high-latitude temperatures (T_I, T_H) and in Figure 6 we show the upper-limit latitudes for the low and intermediate zones (θ_L and θ_I) and the widths of the intermediate- and high-latitude zones ($\theta_I - \theta_L$ and θ_H); recall that, for the equinox insolation case, the upper-limit latitude of the high-zone is $\pi/2$ and the width of the low zone is equivalent to its upper-limit. Over each panel, we indicate the domains that characterize the last-glacial

maximum (G), modern (P) and end-of-the-century future (F) conditions, as discussed in sections 3.1 and 3.2.

The model predictions indicate that the glacial-interglacial changes (G ↔ Pre) and particularly the anthropogenic (Pre ↔ 2019 ↔ F) changes in albedo and greenhouse gases lead to substantial temperature changes (Fig. 5). The temperature of the intermediate-latitude region decreased several degrees between the last glacial and nowadays but may recover back to the glacial levels by the end of the century. The high-latitude region has experienced and will experience much greater changes, progressively warming by several tens of degrees from the past to the present and future conditions.

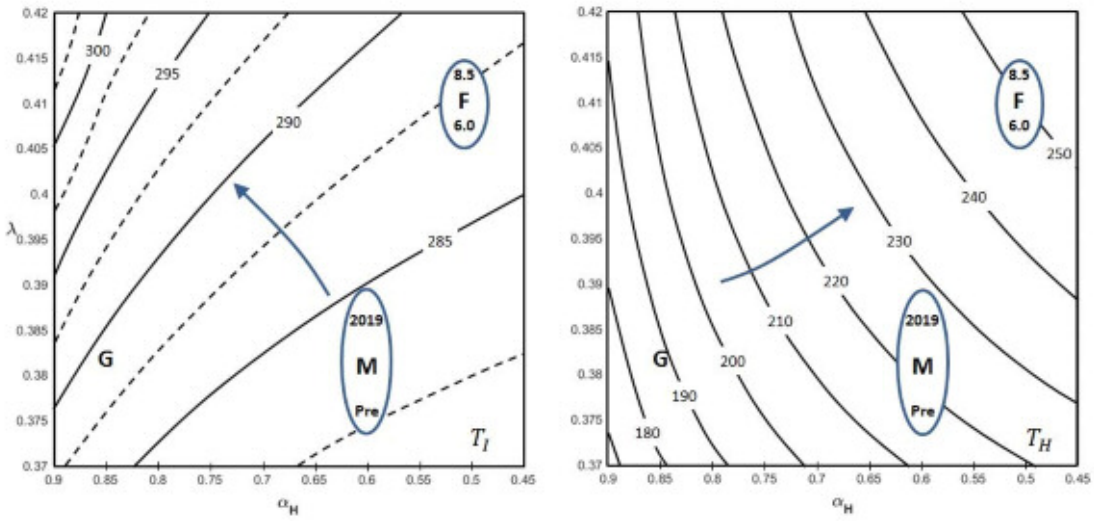

Figure 5. Temperature (K) of the (left panel) intermediate and (right panel) high-latitude zones as a function of high-latitude albedo α_H and greenhouse factor λ. The results correspond to $\alpha_L = 0.30$, $\alpha_I = 0.32$ and $T_L = 300$ K. The symbols indicate the domains that characterize last-glacial-maximum (G), modern (M) and end-of-the-century future (F) conditions, with the arrows indicating the direction of maximum temperature increase.

Regarding the widths of all three zonal bands (Fig. 6), the low-latitude zone shrank slightly between glacial and preindustrial conditions but has progressively expanded since, to enlarge yet several more degrees between nowadays and the end of the century. The intermediate zone expanded substantially (about 0.3 rad or 16°) between the maximum glacial and preindustrial periods but has progressively narrowed since,

and will recover and probably shrink beyond its glacial width by the end of the century. Contrarily, the high-latitude zone retreated some 14° (0.25 rad) between the glacial and preindustrial periods followed by a progressive expansion (and much warming, Fig. 5) that will continue till the end of the century (0.15-0.19 rad or about 9-11° expansion with respect to preindustrial times).

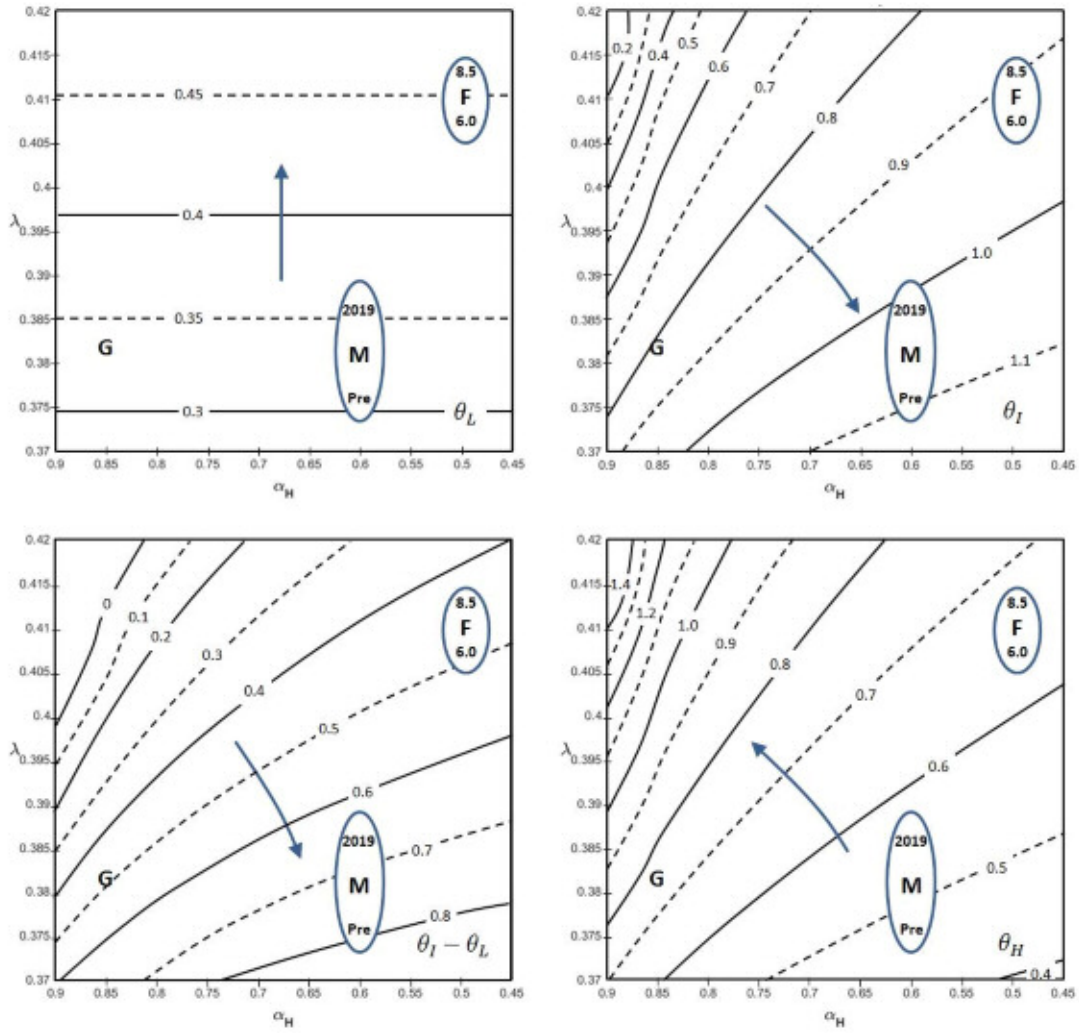

Figure 6. (Top panels) Upper-latitude limits for the low and intermediate zones and (bottom panels) latitudinal widths of the intermediate and high zones, in all cases as a function of high-latitude albedo α_H and greenhouse factor λ (latitudinal values in radians). Recall that the width and upper-limit of the low-latitude zone are equal, and the upper-limit of the high-latitude zone is the North Pole. The results correspond to $\alpha_L = 0.30$, $\alpha_I = 0.32$ and $T_L = 300$ K. The symbols indicate the domains that characterize last-glacial-maximum (G), modern (M) and end-of-the-century future (F) conditions, with the arrows indicating the direction of maximum latitudinal increase.

5. Discussion and concluding remarks

We have developed an idealized three-zone model for each Earth's hemisphere in order to obtain a simplified global energy balance for past, present and future climatic conditions. The latitudinal partition into only three different zones, each with constant temperature, is a major yet realistic simplification. The real Earth has low/high latitude zones that receive more/less solar radiation than is radiated back to the atmosphere, and there is an intermediate zone where the two values are fairly similar. Hence, we choose the intermediate zone to be in radiative balance and set a constant latitudinal energy transport from the low to the intermediate and high zones. The use of constant temperature values for each zone is a major (yet necessary) simplification that reflects the common partition of the Earth's climate into tropical, temperate and polar regions. The model neither considers differences between the northern and southern hemispheres (possibly significant because of the very different land-sea coverage), nor allows any feedback between temperature and the albedo-greenhouse coefficients.

One important feature of the model is that it maximizes the latitudinal energy transport, i.e. the poleward transfer of the tropical radiation surplus is maximum between the low- and intermediate-latitude zones as well as between the intermediate- and high-latitude zones. This is a simple yet very powerful idea that produces two additional equations that allow obtaining a deterministic solution for the latitudinal heat transport as well as the temperatures and widths of all three zones.

In the first part of the paper, we have examined the potential relevance of the Earth's declination in the partitioning of the heat balance. This has led us to realize that the application of the model is conditioned by the way the actual annually-integrated insolation is distributed latitudinally, which is a function of the Earth's declination. For example, periods of high declination would lead to maximum summer and minimum winter incoming radiation at high latitudes of the northern hemisphere, and the opposite for the southern hemisphere. Since the Earth's response is not linear – the outgoing radiation is proportional to the fourth power of the temperature – the actual annually-averaged response will neither correspond to equinox conditions nor to a simple linear average of the annually-varying conditions.

In order to appraise the actual radiative conditions causing the annual-mean values, we have developed a simple procedure that allows estimating an effective declination for both hemispheres. The corresponding zonal temperatures and widths turn out to be similar but not equal to the equinox forcing conditions, with the largest differences occurring in the high-latitude band, hence pointing at a real climatic relevance of the actual declination, e.g. temperature changes at high latitudes would lead to a significant change in albedo, which would in turn affect the temperature, in some sort of positive feedback mechanism. Therefore, we interpret the variations in solar declination as affecting both the greenhouse factor and the high-latitude albedo, and focus on detecting the effects driven by changes in these parameters.

In the second part of the paper, after recognizing the model's idealizations but also realizing its robustness and good potential to detect trends, we have used the equinox forcing conditions to explore the sensitivity of the Earth's heat balance to changes in three parameters: low-zone temperature, high-latitude albedo and greenhouse factor. The probable feedbacks between declination, temperature, ice-coverage and greenhouse gases have led us to examine what is the response of the Earth system to different values of the albedo and greenhouse factor, estimated to represent the last-glacial-maximum, modern and end-of-the century conditions (section 3). In particular, we have developed a simple procedure to calculate the greenhouse factor from known coexisting values of temperature and carbon dioxide concentration (section 3.2).

We find that a warming of the tropical region leads to a large widening of the tropical and intermediate regions, a small warming of the intermediate zone and a large cooling of the high-latitude zone, e.g. when using the 2019 albedo and greenhouse coefficients it turns out that a 3 K tropical change (from 30 $^{\circ}$C to 33 $^{\circ}$C) would produce a 10° widening of the tropical and intermediate regions, a warming of only 2 K in the intermediate regions and a cooling of the high-latitude zone by 15 K (the Earth's mean temperature increases by 1.9 K).

When moving from the last-glacial-maximum to the present and end-of-the-century conditions, the major change corresponds to a large increase in the temperature of the high-latitude zone (38 K from glacial to present and another 20 K by year 2100) (Figs. 5 and 7). During this same period, the widths of the three zones displayed less drastic

yet very compelling changes: the size of the low-latitude zone has remained fairly unchanged till now but will expand some 4° by year 2100; the intermediate zone expanded some 16° till preindustrial times but started to narrow thereafter, and will find again its glacial width by year 2100; and the high-latitude retreated 14° by the preindustrial period, this trend changing thereafter such that it will recover 9-11° by the end of the 21st century (Figs. 6 and 7).

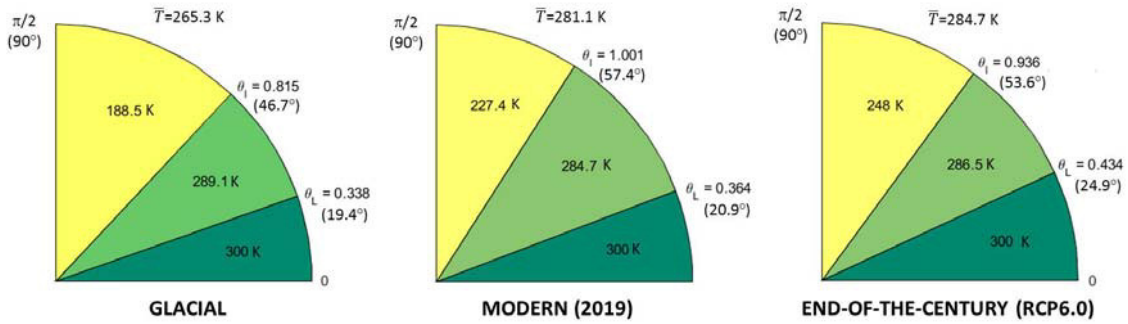

Figure 7. Schematics of the spatial distribution and mean temperatures during (left panel) last-glacial-maximum, (middle panel) present and (right panel) end-of-the-century RCP6.0 conditions. Each panel shows the extension and temperature of each latitudinal zone, as well as the Earth's average temperature.

The Earth's average temperature ($\overline{T}$) for glacial-maximum, present (2019) and end-of-the-century conditions (RCP6.0 scenario) are 265.3 K, 281.1 K and 284.7 K, respectively (Fig. 7). The mean temperatures are below the observations and more refined predictions, and the trends are larger than observed or predicted (Table 1). Nevertheless, in all cases, these trends do reproduce the direction of past and present changes. Keeping in mind the simplicity of our model (it has zero tuning!) and considering that we are using a constant low-latitude temperature and the equinox forcing conditions, we find these results remarkable.

It is important to point out that our predictions are highly dependent on the selection of the low-latitude temperature, high-latitude albedo and greenhouse factor; for example, if we had chosen smaller/larger future greenhouse/albedo values then the predicted changes would have been substantially smaller, allowing a better fit to projections with much more sophisticated models. However, this has not been our objective; rather, we have preferred to focus on determining the trends as a function

of the controlling parameters, particularly on what will be the outcome of the current increase in greenhouse factor and decrease in high-latitude albedo.

The arrows in Figures 6 and 7 indicate, for each variable, which are the directions of maximum change in the $\alpha_H - \lambda$ domain. Remarkably, the pathway for the maximum changes in high-latitude temperature is along the current direction of decreasing albedo and increasing greenhouse factor (Fig. 6), clarifying why the high latitudes of the northern hemisphere are experiencing such a major warming; in the southern hemisphere, the high-latitude albedo has remained more constant so the expected change (which is solely due to λ) is much smaller. In contrast, the temperature of the intermediate zone and the widths of the intermediate- and high-latitude zones have a direction of maximum increase that corresponds to either an increase in λ or a decrease in α_{H} but not both, explaining why the final outcome depends on the relative weight of one factor or another.

Finally, it is worth emphasizing the mitigating effect that a change in the low-latitude temperature (T_L) can have in the projected warming (Fig. 4). We have assumed that T_L remains constant in time but all predictions [18] do show that the equatorial and tropical regions will also warm, yet less than other regions in the globe. Under this situation the low-latitude zone will be able to radiate more energy back to the atmosphere and the energy transport to the intermediate- and high-latitude zones will decrease, leading to a deceleration in the predicted rates of warming.

Our study has two principal underlying ideas. The first one is that the Earth, as any living being, is a complex system that optimizes the distribution of resources, very particularly the heat arriving from the Sun [14,15]. How this is accomplished, i.e. the spatial and temporal patterns that bring about this optimization, falls behind the objectives of our study. However we can use this constructal concept in order to introduce the additional equations that allow solving for the Earth's latitudinal heat transport, as well as for the widths and temperatures of the three-zone Earth's latitudinal partition. The model demonstrates that anthropogenic-induced changes in high-latitude albedo and greenhouse effect add together to moderately expand the size and greatly increase the temperature of the high-latitude regions. The second underlying idea is that the meridional distribution of heat is sensitive to the Earth's

declination. This distribution would produce modifications in the two most remarkable climatic-sensitive parameters, albedo and greenhouse factor, which would have a substantial feedback effect on the temperature and extension of the Earth's climatic zones.

Acknowledgments

This work has been funded by the Spanish Government through projects VA-DE-RETRO (Ministerio de Economía y Competitividad, ref. no. CTM2014-56987-P) and SAGA (Ministerio de Ciencia, Innovación y Universidades, ref. no. RTI2018-100844-B-C33). We wish to thank Samuel Martínez-Pita for his help carrying out the numerical calculations. This article is a publication of the Unidad Océano y Clima of the Universidad de Las Palmas de Gran Canaria, a R+D+I CSIC-associate unit.

References

[1] A. Bejan, Theory of organization in Nature: pulsating physiological processes, Int. J. Heat Mass Transfer, 40 (1997) 2097-2104.

[2] A. Bejan, From heat transfer principles to shape and structure in nature: Constructal theory, J. Heat Transfer Trans. ASME 122 (2000) 430-449.

[3] A. Bejan, S. Lorente, The constructal law of design and evolution in nature, Philos. Trans. R. Soc. Lond. B Biol. Sci. 365 (2010) 1335-1347.

[4] A. Bejan, S. Lorente, The constructal law and the evolution of design in nature, Phys. Life Rev. 8 (2011) 209-240.

[5] A. Bejan, Constructal-theory network of conducting paths for cooling a heat generating volume, Int. J. Heat Mass Transfer 40 (1997) 799-811.

[6] A. Bejan, M.R. Errera, Deterministic tree networks for fluid flow: Geometry for minimal flow resistance between a volume and one point, Fractals 5 (1997) 685-695.

[7] A. Bejan, Shape and Structure, from Engineering to Nature, Cambridge University Press, Cambridge, 324 pp, 2000.

[8] A. Bejan, A.H. Reis, Thermodynamics of optimization of global circulation and climate, Int. J. Energy Res. 29 (2005) 303-316.

[9] A.H. Reis, A. Bejan, Constructal theory of global circulation and climate, Int. J. Heat Mass Transfer 49 (2006) 1857-1875.

[10] M. Clausse, F. Meunier, A.H. Reis, A. Bejan, Climate change, in the framework of the constructal law, Int. J. Global Warming 4 (2012) 242-260.

[11] H. Stommel, Thermohaline convection with two stable regimes of flow, Tellus, 13 (1961) 224–230.

[12] H. Stommel, C. Rooth, On interaction of gravitational and dynamic forcing in simple circulation models, Deep-Sea Res. 15 (1968) 165-170.

[13] R.X. Huang, J.R. Luyten, H.M. Stommel, Multiple equilibrium states in combined thermal and saline circulation, J. Phys. Oceanogr. 22 (1992) 231-246.

[14] J.L. Pelegrí, A physiological approach to oceanic processes and glacial-interglacial changes in atmospheric CO_2, Sci. Mar. 72 (2008) 125–202.

[15] J.L. Pelegrí, P. De La Fuente, R. Olivella, A. García-Olivares, Global constraints on net primary production and inorganic carbon supply during glacial and interglacial cycles, Paleoceanogr. 28 (2013) 713-725.

[16] A. Gill, Atmosphere-Ocean Dynamics, Academic Press, San Diego, 662 pp, 1982.

[17] J.P. Peixoto, A.H. Oort, Physics of Climate, Springer-Verlag, New York, 520 pp, 1992.

[18] M. Collins, R. Knutti, J. Arblaster et al., Long-term climate change: projections, commitments and irreversibility, in Climate Change 2013: The Physical Science Basis, contribution of Working Group I to the Fifth Assessment Report of the Intergovernmental Panel on Climate Change, edited by T.F. Stocker, et al., pp. 1029-1136, Cambridge University Press, Cambridge, U.K., and New York, NY, USA, 2013.

[19] J. Hansen, R. Ruedy, M. Sato, K. Lo, Global surface temperature change, Rev. Geophys. 48 (2010) RG4004.

[20] N. Lenssen, G. Schmidt, J. Hansen, M. Menne, A. Persin, R. Ruedy, D. Zyss, Improvements in the GISTEMP uncertainty model, J. Geophys. Res. Atmos. 124 (2019) 6307-6326.

[21] C. Le Quére, R.M. Andrew, P. Friedlingstein, et al., Global carbon budget 2018, Earth Syst. Sci. Data, 10 (2018) 2141-2194.

[22] D.W. Fahey, S.J. Doherty, K.A. Hibbard, A. Romanou, P.C. Taylor, Physical drivers of climate change, in Climate Science Special Report: Fourth National Climate Assessment, Volume I, edited by D.J. Wuebbles, et al., pp. 73-113, U.S. Global Change Research Program, Washington, DC, USA, 2017.

[23] H.G. Houghton, Physical Meteorology, MIT Press, Cambridge, MA, 442 pp, 1985.

[24] J.R. Hummel, R. Reck, A global surface albedo model, J. Appl. Meteor. 18 (1979) 239-253.

[25] F. Bender, H. Rodhe, R.J. Charlson, A.M.L. Ekman, N. Loeb, 22 views of the global albedo – Comparison between 20 GCMs and two satellites, Tellus 58A (2006), 320–330.

[26] R.T. Pierrehumbert, Principles of Planetary Climate, Cambridge University Press, Cambridge, U.K., and New York, NY, USA, 652 pp, 2010.

[27] G.L. Stephens, The albedo of Earth, Rev. Geophys. 53 (2015) 141-163.

[28] O. Andry, R. Bintanja, W. Hazeleger, Time-dependent variations in the Arctic's surface albedo feedback and the link to seasonality in sea ice, J. Climate 30 (2017) 393-410.

[29] R. Ellis, M. Palmer, Modulation of ice ages via precession and dust-albedo feedbacks, Geosc. Frontiers 7 (2016) 891e909.

[30] K.E. Trenberth, J.F. Fasullo, J. Kiehl, Earth's global energy budget, Bull. Amer. Meteorol. Soc. 3 (2009) 311-323.

[31] G.L. Stephens, J. Li, M. Wilde, et al., An update on Earth's energy balance in light of the latest global observations, Nature Geosc. 5 (2012) 691-696.

[32] A.McC. Hogg, Glacial cycles and carbon dioxide: A conceptual model, Geophys. Res. Lett. 35 (2008) L01701.

[33] V. Ramaswamy, O. Boucher, J. Haigh, D. Hauglustaine, J. Haywood, G. Myhre, T. Nakajima, G. Shi, S. Solomon, Radiative forcing of climate change, in Climate Change 2001: The Scientific Basis, edited by J. T. Houghton, et al., pp. 350-406, Cambridge Univ. Press, New York, 2001.

[34] J.R. Petit, J. Jouzel, D. Raynaud, et al., Climate and atmospheric history of the past 420000 years from the Vostok ice core, Antarctica, Nature 399 (1999) 429-436.

[35] D. Lüthi, M. Le Floch, B. Bereiter et al., High-resolution carbon dioxide concentration record 650,000–800,000 years before present, Nature 378 (2008) 379–382.

[36] D. Rind, D. Peteet, Terrestrial conditions at the last glacial maximum and CLIMAP sea-surface temperature estimates: are they consistent? Quaternary Res. 24 (1985) 1-22.

[37] T. Schneider von Deimling, A. Ganopolski, H. Held, S. Rahmstorf, How cold was the Last Glacial Maximum? Geophys. Res. Lett. 33 (2006) L14709.

[38] G. Feulner, S. Rahmstorf, A. Levermann, S. Volkwardt, On the origin of the surface air temperature difference between the hemispheres in Earth's present-day climate, J. Climate 26 (2013) 7136-7150.

[39] J.W.H. Weijers, E. Schefuß, S. Schouten, S. Damsté, Coupled thermal and hydrological evolution of tropical Africa over the last deglaciation, Science Rep. 315 (2007) 1701-1704.

[40] T. McKnight, D. Hess, Climate Zones and Types, in Physical Geography, A Landscape Appreciation, Chapter 8, Prentice Hall, 6th edition, 2000.

[41] K.E. Trenberh, J.M. Caron, Estimates of meridional atmosphere and ocean heat transports, J. Climate 14 (2001) 3433-3443.